COBEM UBERLÂNDIA 2019

ABCM Associação Brasileira de Engenharia e Ciências Mecânicas

25th ABCM International Congress of Mechanical Engineering
October 20-25, 2019, Uberlândia, MG, Brazil

COB-2019-1641
COMPARISON OF TWO SLIDING MODE CONTROL TECHNIQUES APPLIED TO A ROV VERTICAL MOTION.

Reginaldo Cardoso
Éverton Lins de Oliveira
Décio Crisol Donha
Mechanical Engineering Department, University of São Paulo, Brazil
reginaldo.cardoso85@gmail.com; ev_lins@hotmail.com; dcdonha@usp.br

Abstract. *This paper presents the comparison of two alternative sliding mode control techniques used to control the motion of an ROV in the azimuthal plane. The first one is based in a classical method, where it is necessary to divide the multivariable system into two SISO systems, and a sliding surface is designed for each input. The other technique is based on zero allocation made by the generalization of the Ackermann's formula. Both techniques demonstrated to be capable of tracking the desired trajectory. The multivariable control law has shown a faster convergence to zero, and both techniques presented similar control effort.*

Keywords: *Sliding mode control, nonlinear control, ROV*

1. INTRODUCTION

Remotely operated vehicles (ROV's) have been used in several research areas, such as operation in depth water to explore the seas and oceans (Khadhraoui *et al.*, 2016).

In general, ROV's are modeled by nonlinear coupled system, with parametric uncertainties and unmodeled dynamics. For this reason, several robust control techniques have been applied to solve its control problems (Ramírez-rodríguez *et al.*, 2017).

Several works used sliding mode control (SMC) (Chen *et al.*, 2016) due to the following advantages: insensitivity to parameter variations and / or model uncertainties and external disturbance rejection (Eker and Akınal, 2008; Utkin and Young, 1978). Furthermore, the performance of SMC is associate with a proper choice of the sliding surface (Utkin *et al.*, 1999). Therefore, it was decided to highlight two techniques that obtain sliding surfaces.

The first technique is a classical method, which was first presented by Yoerger and Slotine (1985). The surface exhibits the dynamic characteristic of a low-pass filter, and the system has to be single-input single-output (SISO). For multi-input multi-output (MIMO) systems are necessary to design one surface to each control input.

Another way to design a sliding surface is based on the generalized multivariable *Ackermann's* formula. According to Young *et al.* (1977), the eigenvalues of the system after the SMC application are equal to the transmission zeros of the original system, thus, the sliding surface construction is solved with zero allocation system.

The purpose of this article is to compare these two techniques of sliding surface design in the vertical ROV model. This paper is divided into: section 2., where the mathematical model (in the azimuthal plane) is presented. Section 3. presents the sliding modes control. The section 4. presents the numerical simulation. Finally, section 5. presents the conclusion and comments.

2. Mathematical Model

In this paper, it will be studied the vertical movement of the ROV with two degrees of freedom as shown in Fig. 1: heave (downward in z axis) and pitch (rotation around the y axis). It will be ignored the influence of the horizontal motion, only the constant velocity (**U**) along the x axis will be considered.

The vehicle was designed with a negative buoyancy force ($34N$), so that if it suffers some failure, it can be easily rescued (Ferreira *et al.*, 2013, 2014). The vehicle can also be seen in Fig. 1.

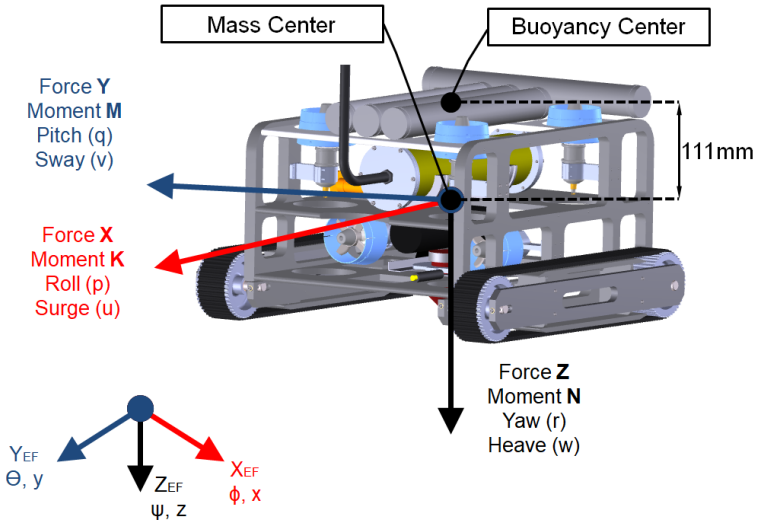

Figure 1. Coordinate system.

According to Chen *et al.* (2016) the equation which describes the ROV model is as follows:

$$\begin{bmatrix} \dot{w} \\ \dot{q} \\ \dot{z} \\ \dot{\theta} \end{bmatrix} = \begin{bmatrix} -\dfrac{(Z_w + Z_{ww}|w|)}{Z_{\dot{w}} - m} & \dfrac{\mathbf{U}(X_{\dot{u}} - m)}{Z_{\dot{w}} + m} & 0 & 0 \\ \dfrac{\mathbf{U}(X_{\dot{u}} - m)}{I_y + M_{\dot{q}}} & \dfrac{(M_q + M_{qq}|q|)}{I_y + M_{\dot{q}}} & 0 & 0 \\ \cos(\theta) & 0 & 0 & 0 \\ 0 & 1 & 0 & 0 \end{bmatrix} \begin{bmatrix} \dot{w} \\ \dot{q} \\ \dot{z} \\ \dot{\theta} \end{bmatrix} + \begin{bmatrix} -\dfrac{1}{Z_{\dot{w}} - m} & 0 \\ 0 & \dfrac{1}{I_y - M_{\dot{q}}} \\ 0 & 0 \\ 0 & 0 \end{bmatrix} \begin{bmatrix} Z \\ M \end{bmatrix} + \begin{bmatrix} \dfrac{\cos(\theta)(\rho_{A,g} - mg)}{Z_{\dot{w}} - m} \\ \dfrac{\rho_{A,g} z b \sin(\theta)}{I_y - M_{\dot{q}}} \\ 0 \\ 0 \end{bmatrix} \tag{1}$$

or,

$$\begin{bmatrix} \dot{\boldsymbol{\nu}} \\ \dot{\boldsymbol{\eta}} \end{bmatrix} = \begin{bmatrix} -\boldsymbol{M}^{-1}(\boldsymbol{C}(\boldsymbol{\nu}) + \boldsymbol{D}(\boldsymbol{\nu})) & \mathbf{0}_{2\times2} \\ \boldsymbol{J}(\boldsymbol{\eta}) & \mathbf{0}_{2\times2} \end{bmatrix} \begin{bmatrix} \boldsymbol{\nu} \\ \boldsymbol{\eta} \end{bmatrix} + \begin{bmatrix} \boldsymbol{M}^{-1} \\ \mathbf{0}_{2\times2} \end{bmatrix} \begin{bmatrix} Z \\ M \end{bmatrix} + \begin{bmatrix} -\boldsymbol{M}^{-1}\boldsymbol{g}(\boldsymbol{\eta}) \\ \mathbf{0}_{2\times1} \end{bmatrix} \tag{2}$$

which can be rewritten as

$$\begin{aligned} \dot{w} &= f_1(w, q, \theta, \mathbf{U}) + b_1 Z \\ \dot{q} &= f_2(w, q, \theta, \mathbf{U}) + b_2 M \\ \dot{z} &= f_3(w, q, \theta, \mathbf{U}) \\ \dot{\theta} &= f_4(w, q, \theta, \mathbf{U}) \end{aligned} \tag{3}$$

where $\boldsymbol{\nu} = \begin{bmatrix} w & q \end{bmatrix}^T$; $\boldsymbol{\eta} = \begin{bmatrix} z & \theta \end{bmatrix}^T$; matrix $\boldsymbol{M}$ represents the sum of the rigid-body mass and the inertia matrix; $\boldsymbol{C}(\boldsymbol{\nu})$ the sum of rigid-body Coriolis and the centripetal matrix with the mass; $\boldsymbol{D}(\boldsymbol{\nu})$ the hydrodynamic damping; $\boldsymbol{g}(\boldsymbol{\eta})$ force vector and gravitational moment and buoyancy; $\begin{bmatrix} Z & M \end{bmatrix}^T$ the control force and the moment vector.

The vehicle mass is $142kg$. The distance between the center of mass and the buoyancy center is 0.111mm, which provides intrinsic stability in roll and pitch to the vehicle. It was used constant drag coefficients in the range of velocities from 0 to $1m/s$ (Ferreira *et al.*, 2014).

Pitch angle (approximately $-2°$) appears when the surge velocity is consider constant and the thrusters are out of symmetry.

3. Sliding Mode Control

The main idea of this paper is the comparison of two strategies for the design of the sliding surface in the sliding mode control.

3.1 SISO Sliding Mode Control (SISO SMC)

The surfaces were chosen according to (Slotine and Li, 1991), which are described as a constant gain multiplied by an error vector.

For this particular application, it has been decided to use the desired velocity equal to zero, because of that, the input control will force the ROV velocity to be as small as possible. The surfaces can be seen in Eq. (4) and Eq. (5),

$$s_1 = -\lambda_1 w + \lambda_2 z_d - \lambda_2 z \tag{4}$$

$$s_2 = -\lambda_3 q + \lambda_4 \theta_d - \lambda_4 \theta \tag{5}$$

where $\lambda_{1,2,3,4}$ are the control bandwidths and z_d, θ_d are the desired trajectories.

The next step is to design an equivalent control, which is responsible to keep the system under the switch surface. The equivalent control is obtained by the derivation of the surface and then the Eq. (3) is applied,

$$\dot{s}_1 = \lambda_2 \dot{z}_d - \lambda_1 \left(f_1 + b_1 Z\right) - \lambda_2 f_3 = 0 \tag{6}$$

$$\dot{s}_2 = \lambda_4 \dot{\theta}_d - \lambda_3 \left(f_2 + b_2 M\right) - \lambda_4 f_4 = 0 \tag{7}$$

the control variables (Z and M) are isolated to obtain the equivalent control (Z_{eq} and M_{eq})

$$Z_{eq} = \frac{\lambda_2 \dot{z}_d - \lambda_2 f_3 - \lambda_1 f_1}{\lambda_1 b_1} \tag{8}$$

$$M_{eq} = \frac{\lambda_4 \dot{\theta}_d - \lambda_4 f_4 - \lambda_3 f_2}{\lambda_3 b_2}. \tag{9}$$

In order to present certain robustness to the control input, it is necessary to add to the equivalent control a discontinuous control, which is responsible to converge the system from the initial instant to the sliding surface.

The discontinuous term depends on the sliding surface and because of that, the control signal can present high-frequency chattering. According to Slotine and Li (1991), it is possible to avoid this chattering by designing a region around the sliding surface, where the discontinuous control does not change. This region is named as boundary layer ($\phi_{1,2}$). Thus, the control law can be described,

$$Z = -\frac{K_1}{\lambda_1 b_1} sat\left(\frac{s_1}{\phi_1}\right) - Z_{eq} \tag{10}$$

$$M = -\frac{K_2}{\lambda_3 b_2} sat\left(\frac{s_2}{\phi_2}\right) - M_{eq} \tag{11}$$

where $K_{1,2}$ are the control gains.

In the SISO SMC project - Eq. (10) and Eq. (11) - some parameters, such as $\lambda_{1,2,3,4}$, $K_{1,2}$ and $\phi_{1,2}$, which need to be defined and adjusted.

The λ parameter have to obey the following relation $\lambda < \frac{1}{5} S_R$, where S_R is the sampling rate (Slotine and Li, 1991). In the simulation, the sampling rate was used equal $100Hz$, therefore $\lambda_{1,2,3,4} = 20$.

To adjust the boundary layer is necessary to specify an acceptable error. In this case, it was defined $10cm$ ($E_z = 0.1m$) in the linear position and 1° ($E_\theta = 1^\circ$) in the angular position, thus

$$\phi_1 = \lambda E_z \;\rightarrow\; \phi_1 = 20\, 0.1 = 2 \tag{12}$$

$$\phi_2 = \lambda E_\theta \;\rightarrow\; \phi_2 = 20\, \frac{\pi}{180} 1 = 0.349. \tag{13}$$

The controller gains ($K_{1,2}$), were obtained with the sliding condition (Slotine and Li, 1991). This condition is responsible to make all trajectories outside from the sliding surface to converge to the surface.

The following function, $\boldsymbol{V}(s) = \frac{1}{2} s^2$, can be chosen as *Lyapunov* function. The derivative of the *Lyapunov* function must be negative-defined to ensure surface stability,

$$\dot{V} = \dot{s} s \leq -\gamma |s| \tag{14}$$

where γ is a positive constant and it can be defined,

$$t_{reach} \leq \frac{|s(0)|}{\gamma} \rightarrow \gamma \leq \frac{|s(0)|}{t_{reach}} \tag{15}$$

where t_{reach} is the desired time for the system to reach the sliding surface.

The initial conditions are $[w(0) = 0, q(0) = 0, z(0) = 5, \theta(0) = 2^\circ]$ and $t_{reach} = 10s$. Therefore, $|s_1(0)| = 100$, $|s_2(0)| = 100^\circ$, $\gamma_1 = 10$ and $\gamma_2 = 10^\circ = 0.175rad$.

Applying the Eq. (10) into Eq. (6) and the Eq. (11) into Eq. (7),

$$\dot{s}_1 = K_1 sat\left(\frac{s_1}{\phi_1}\right) \tag{16}$$

$$\dot{s}_2 = K_2 sat\left(\frac{s_2}{\phi_2}\right). \tag{17}$$

The next step is to replace Eq. (16) and Eq. (17) in the derivative of the *Lyapunov* function Eq. (14)

$$\begin{aligned} K_1 sat\left(\frac{s_1}{\phi_1}\right) s_1 &\leq -\gamma_1 |s_1| \\ K_1 &\leq \gamma_1 = \frac{100}{10} = 10 \end{aligned} \tag{18}$$

$$\begin{aligned} K_2 sat\left(\frac{s_2}{\phi_2}\right) s_2 &\leq -\gamma_2 |s_2| \\ K_2 &\leq \gamma_2 = \frac{1.745}{10} = 0.175. \end{aligned} \tag{19}$$

3.2 MIMO Sliding Mode Control (MIMO SMC)

To simplify the design of the controller is necessary to rewrite the Eq. (2). This new representation is divided into nonlinear and linear parameters, such as the Eq. (20)

$$\dot{\boldsymbol{x}} = (\boldsymbol{A} + \boldsymbol{\Delta A})\boldsymbol{x} + \boldsymbol{B\tau} + (\boldsymbol{G} + \boldsymbol{\Delta G}), \tag{20}$$

where $\boldsymbol{x} = [\boldsymbol{\nu} \quad \boldsymbol{\eta}]^T$ and the nonlinearities are represented by $\boldsymbol{\Delta A}$ and $\boldsymbol{\Delta G}$.

According to Cardoso *et al.* (2017), the sliding surface can be obtained by the zeros allocations. This technique is based on the generalization of the *Ackermann's* formula, which shows that the poles of the sliding mode surface are equals to the zeros of the open-loop system (Utkin and Young, 1978) (Utkin *et al.*, 1999).

According to Meza and Bhaya (2001), it is possible to allocate the zeros by changing the original system representation to the canonical form of *Luenberger*, thus the zeros allocation can be solved by inspection.

The first step is to transform the original system into the *Hessenberger* form, and obtain the controllability indices of the linearized system. After some algebraic manipulations, the *Luenberger* form is obtained. Therefore, the system transformation matrices ($\boldsymbol{T}$ and $\boldsymbol{U}$) are obtained.

The matrix ($\boldsymbol{C}$) is the zeros allocation, which can be named as switching matrix. The system transformation process and the zeros allocation can be viewed in the flow chart in Fig. 2. More details can be seen at Meza and Bhaya (2001) and Meza (1999).

The sliding surface ($\boldsymbol{s}$) can be written as,

$$\boldsymbol{s} = \boldsymbol{C}(\boldsymbol{x} - \boldsymbol{x}_d) \tag{21}$$

where $\boldsymbol{x}_d$ is the desired position of the vehicle.

The equivalent control can be designed by deriving the Eq. (21),

$$\dot{\boldsymbol{s}} = \boldsymbol{C}\dot{\boldsymbol{e}} = \boldsymbol{C}(\dot{\boldsymbol{x}} - \dot{\boldsymbol{x}}_d) = \boldsymbol{0}. \tag{22}$$

Before proceeding with the control development, it is necessary to treat the nonlinearities. Therefore, it is assumed that the nonlinearities are limited, such as Eq. (23) (Cardoso *et al.*, 2017),

$$\begin{aligned} \boldsymbol{\Delta A} &= \boldsymbol{BH}, \quad \|\boldsymbol{H}\| \leq \beta_1 \\ \boldsymbol{\Delta G} &= \boldsymbol{BF}, \quad \|\boldsymbol{F}\| \leq \beta_2. \end{aligned} \tag{23}$$

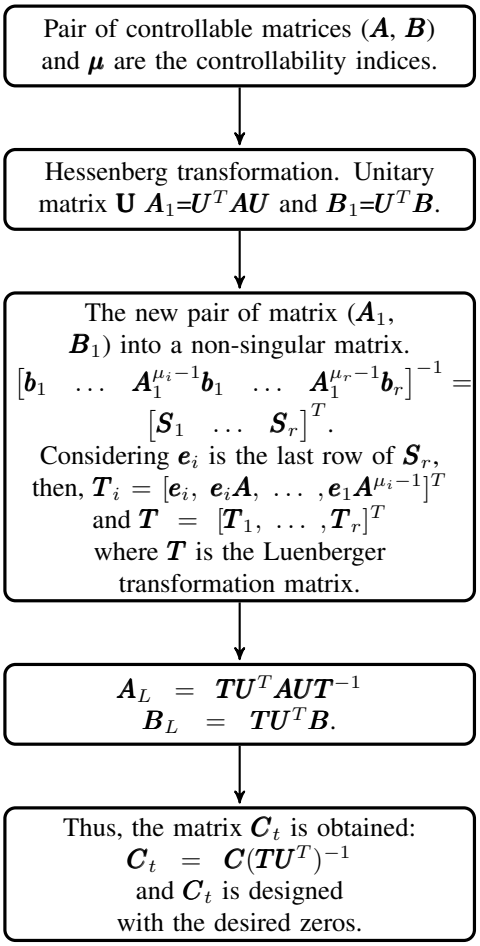

Figure 2. Flow chart of *Luenberger* transformation and the zeros allocations (Meza and Bhaya, 2001).

Applying Eq. (20) and Eq. (23) into Eq. (22), and isolating the variable $\tau = \tau_{eq}$

$$\tau_{eq} = -\|(\boldsymbol{C}\boldsymbol{B})^{-1}\boldsymbol{C}\boldsymbol{A}\|\|\boldsymbol{x}\| - \|(\boldsymbol{C}\boldsymbol{B})^{-1}\boldsymbol{C}\boldsymbol{G}\| + \|(\boldsymbol{C}\boldsymbol{B})^{-1}\boldsymbol{C}\|\|\dot{\boldsymbol{x}}_d\| - \beta_1\|\boldsymbol{x}\| - \beta_2. \tag{24}$$

The control law was chosen according to (Hsu, 1998) and (Cardoso *et al.*, 2017). It was based on the following *Lyapunov* function, $V = 1/2\|\boldsymbol{s}\|^2$. The system will be asymptotically stable if the following condition Eq. (25) is obeyed

$$\dot{\boldsymbol{V}} = \boldsymbol{s}^T\dot{\boldsymbol{s}} < 0. \tag{25}$$

To satisfy this condition Eq. (25), the following control law is obtained

$$\begin{aligned} \boldsymbol{\tau} &= \frac{\beta}{h}\tau_{eq}\boldsymbol{\alpha} \\ \boldsymbol{\alpha} &= -\frac{\boldsymbol{B}^T\boldsymbol{C}^T\boldsymbol{s}}{\phi_3 + \|\boldsymbol{B}^T\boldsymbol{C}^T\boldsymbol{s}\|}. \end{aligned} \tag{26}$$

where h is a positive constant, $\beta > 0$ and ϕ_3 is the boundary layer, which was used to avoid a chattering action in the input control. The control input ($\boldsymbol{\tau}$) is a vector with size $\Re^{2\times 1}$.

Applying Eq. (26) and Eq. (24) into Eq. (25)

$$\dot{V} = \|\boldsymbol{s}^T\boldsymbol{B}\boldsymbol{C}\|\tau_{eq}(-1 + \frac{\beta}{(h)^2}) < 0. \tag{27}$$

the (27) will always be true if the following two conditions are obeyed: $h^2 > \beta$ and $\beta > 0$.

Comparing Eq. (10) and Eq. (11) with Eq. (26), these equations have the same structure thus, these can be rewritten as Eq. (28)

$$\begin{aligned} Z &= K_1\tau_{eq}\boldsymbol{\alpha}(1) \\ M &= K_2\tau_{eq}\boldsymbol{\alpha}(2) \end{aligned} \tag{28}$$

with $K_1 = 110/11 = 10$ and $K_2 = 1.75/10 = 0.175$. However, it is possible to use the same controller gain of Eq. (10) and Eq. (11) to satisfy the condition Eq. (27).

The matrices values ($\boldsymbol{C}_t$ and $\boldsymbol{C}$) are shown in Eq. (29),

$$\boldsymbol{C}_t = \begin{bmatrix} 1 & 2 & 0 & 0 \\ 0 & 0 & 1 & 1 \end{bmatrix}, \boldsymbol{C} = \begin{bmatrix} 2.681 & 0 & 5.362 & 0 \\ 0 & 6.105 & 0 & 6.105 \end{bmatrix}, \tag{29}$$

the values in $\boldsymbol{C}_t$ represents the zeros allocation, $(s+2) \rightarrow zero = -2$ and $(s+1) \rightarrow zero = -1$, these were obtained after an exhaustive search. The same procedure was used to obtained the boundary layer value ($\phi_3 = 0.02$).

3.3 Merge control

After some simulations, it was noticed the existence of a steady-state error in θ with the MIMO SMC, which can be seen at Fig. 4 (the black curve). This happened because of the equivalent control, calculated in Eq. (24). As the same error did not happen in the SISO SMC, it was decided to merge the two techniques (MIMO discontinuous control was applied to SISO control law).

Comparing the λ and matrix $\boldsymbol{C}$ values, it can be inferred that $\lambda_3 = 6.105$ and $\lambda_4 = 6.105$, thus

$$\begin{aligned} Z &= K_1 \tau_{eq} \boldsymbol{\alpha}(1) \\ M &= K_2 \boldsymbol{\alpha}(2) + \left[\frac{\lambda_4 \dot{\theta}_d - \lambda_4 f_4 - \lambda_3 f_2}{\lambda_3 b_2} \right]. \end{aligned} \tag{30}$$

4. Simulation

The ROV constant velocity was chosen as $\mathbf{U} = 0.9m/s$. The parameters used to simulate can be found in table 1.

Table 1. Vehicle and controls parameters.

Parameter	Value	Parameter	Value	SISO SMC	MIMO SMC	Merge Control
m	142 Kg	I_y	19.79 Kgm^2	$K_1 = 10$	$K_1 = 10$	$K_1 = 10$
mg	1391.6 N	Z_w	311.64Kg/s	$K_2 = 0.175$	$K_2 = 0.175$	$K_2 = 550$
$\rho_{A,g}$	1424.92 N	M_q	-5Kgm^2/(srad)	$\lambda_{1,2,3,4} = 20$	$zero = -2$	$\lambda_{3,4} = 6.105$
$X_{\dot{u}}$	-450.5 Kg	$Z_{w\|w\|}$	-1706.55Kg/m	$\phi_1 = 2$	$zero = -1$	$\phi_3 = 0.02$
$Z_{\dot{w}}$	-550 Kg	$M_{q\|q\|}$	-200Kgm^2/rad^2	$\phi_2 = 0.349$	$\phi_3 = 0.02$	-
$M_{\dot{q}}$	-200 Kgm^2	zb	-0.11m	-	-	-
Z	-562.890/881.588 N	M	-230.394/230.394 Nm	-	-	-

The desired trajectory in z was defined by a sinusoidal function with low frequency ($f = 0.01Hz$) and an amplitude ($Amp = 5m$), in consequence of that, the actuators did not reach saturation during the simulation.

$$\begin{aligned} z_{desired}(t) &= Amp \sin(2\pi f t) + b \\ \theta_{desired}(t) &= 0 \end{aligned} \tag{31}$$

where $b = 10$, which was chosen to be different from the initial condition.

Figure 3 present the linear position errors, it is possible to observe that MIMO SMC error (z) converge to zero faster than the SISO SMC (approximately 10s). The zoom box exhibits that MIMO has not oscillation in the steady-state. The merge control (curve in magenta) has the same response of the MIMO SMC because Z input on both controls is the same.

According to Fig. 4, the merge control converges to zero (in approximately 3s), which is faster than the others techniques. On the other hand, MIMO SMC presents a steady-state error, approximately $0.05°$. This error may has occurred due to the equivalent control design since it was assumed that nonlinearities were limited (23).

Figure 5 (Z force) and Fig. 6 (M moment) present the control efforts. After the first 10s of simulation, the differences between all techniques are indistinguishable. Besides that, in the first 10s, the Z force reached the actuator saturation.

The MIMO sliding surface needed to be split into two surfaces in order to be compared to SISO Fig. 7 and Fig. 8 present comparison between MIMO and SISO sliding surfaces.

According to Fig. 8, MIMO surface converges to zero 1 second before SISO.

5. Conclusion

The synthesized sliding mode controllers were able to make the vehicle tracks the desired trajectory. The MIMO SMC has advantages over SISO SMC because with the same control effort presented a faster response without steady-state error in z.

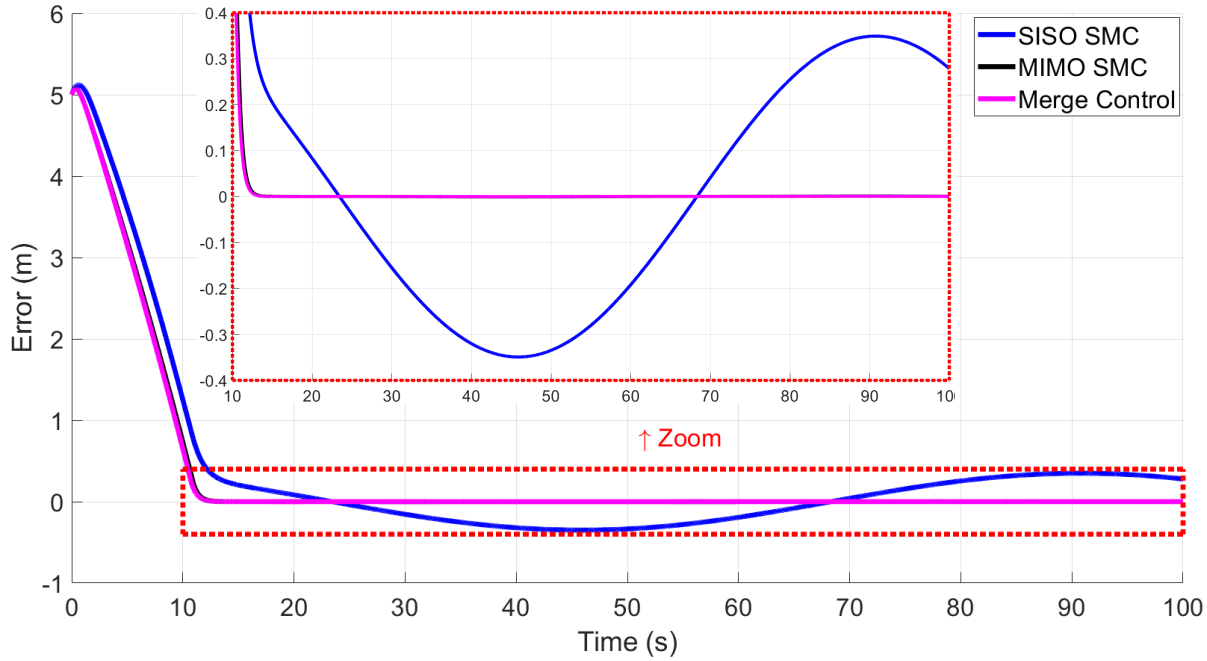

Figure 3. The error between the desired and real trajectory, for each control techniques.

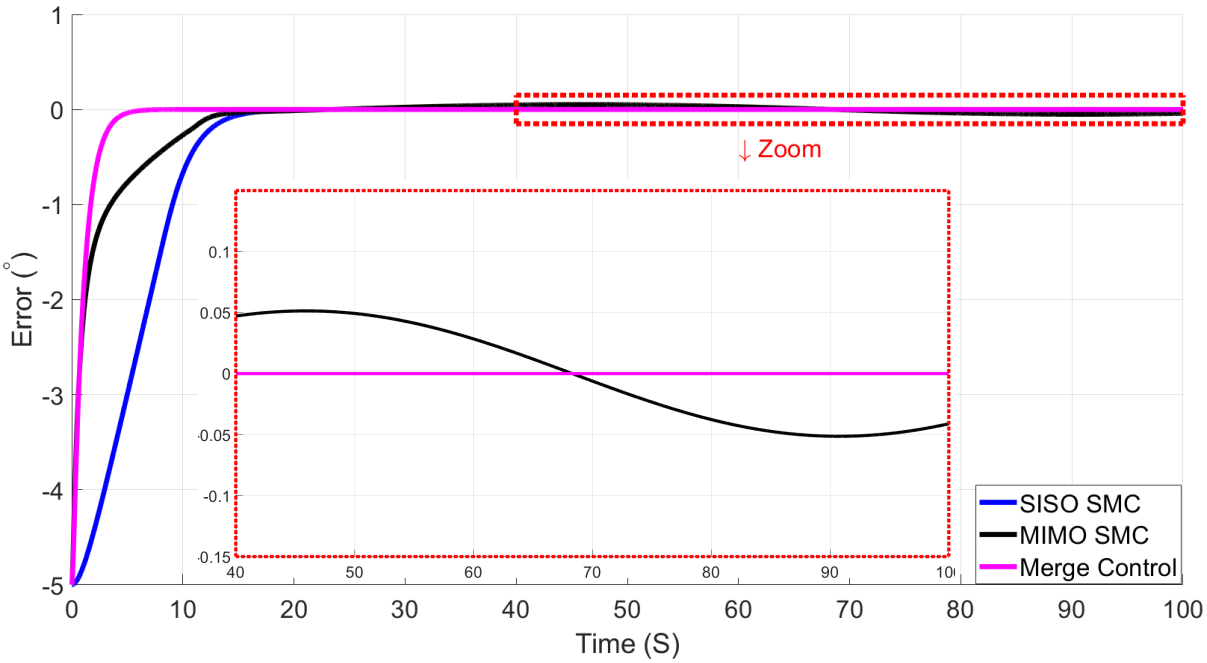

Figure 4. The error between the desired and real angular position, for each control techniques.

In spite of that, MIMO SMC presented an oscillatory response in θ (between $0.05°$ and $-0.05°$), which was caused by the equivalent control design. This oscillation is not irrelevant when compared to the vehicle dimensions (length$=$ 1076mm, width$=$ 852mm, and height$=$ 705mm).

The oscillatory response did not happen in the merge control because it was decided to combine the SISO equivalent control with the MIMO control law.

6. REFERENCES

Cardoso, R., Meza, M.E.M., Rafikova, E. and Titotto, S.L.M.C., 2017. "Backstepping and integrative sliding mode control for trajectory tracking of a hybrid remotely operated vehicle". In *2017 IEEE International Conference on Robotics and Biomimetics (ROBIO)*. pp. 116–121. doi:10.1109/ROBIO.2017.8324404.

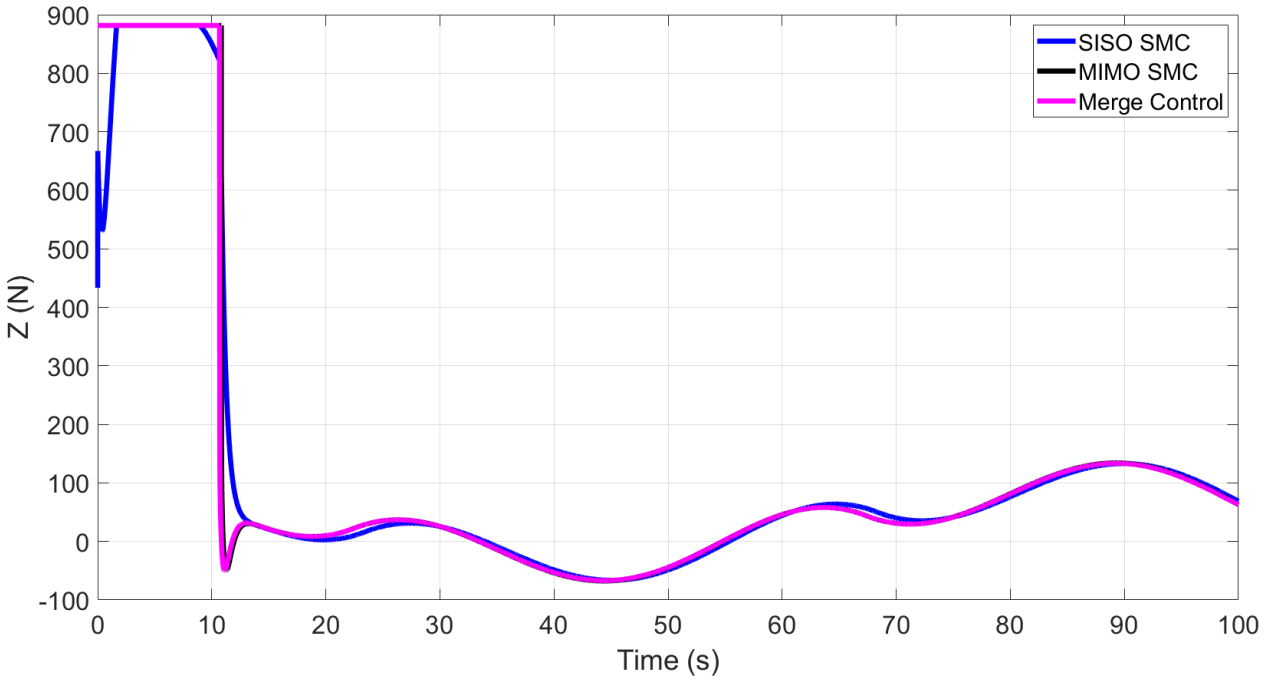

Figure 5. Effort control Z.

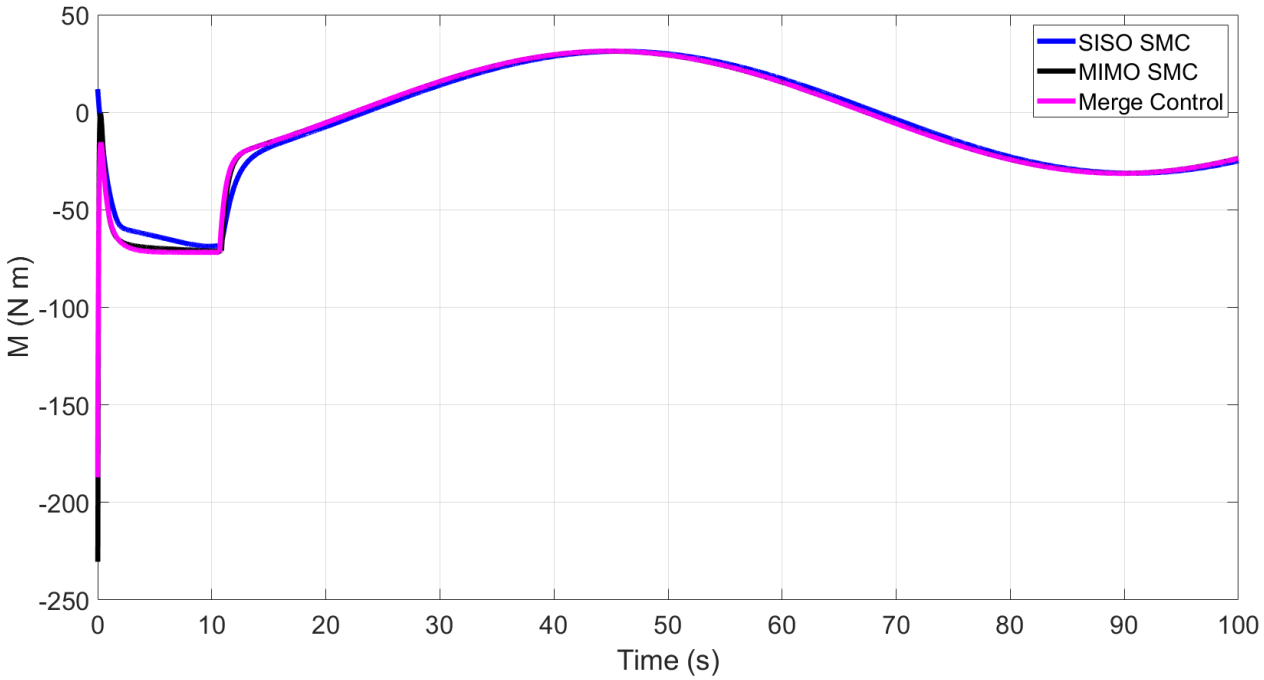

Figure 6. Effort control M.

Chen, W., Wei, Y., Liu, H. and Zhang, H., 2016. "Bio-inspired sliding mode controller for ROV with disturbance observer". *2016 IEEE International Conference on Mechatronics and Automation, IEEE ICMA 2016*, pp. 599–604. doi:10.1109/ICMA.2016.7558631.

Eker, l. and Akınal, u.A., 2008. "Sliding mode control with integral augmented sliding surface: design and experimental application to an electromechanical system". *Electrical Engineering*, Vol. 90, No. 3, pp. 189–197. ISSN 0948-7921. doi:10.1007/s00202-007-0073-3.

Ferreira, C.Z., Conte, G.Y.C., Avila, J.P.J., Pereira, R.C. and Ribeiro, T.M.C., 2013. "Underwater robotic vehicle for ship hull inspection: control system architecture". In *COBEM: 22nd International Congress of Mechanical Engineering, 2013*. pp. 1231–1241. ISSN 2176-5480.

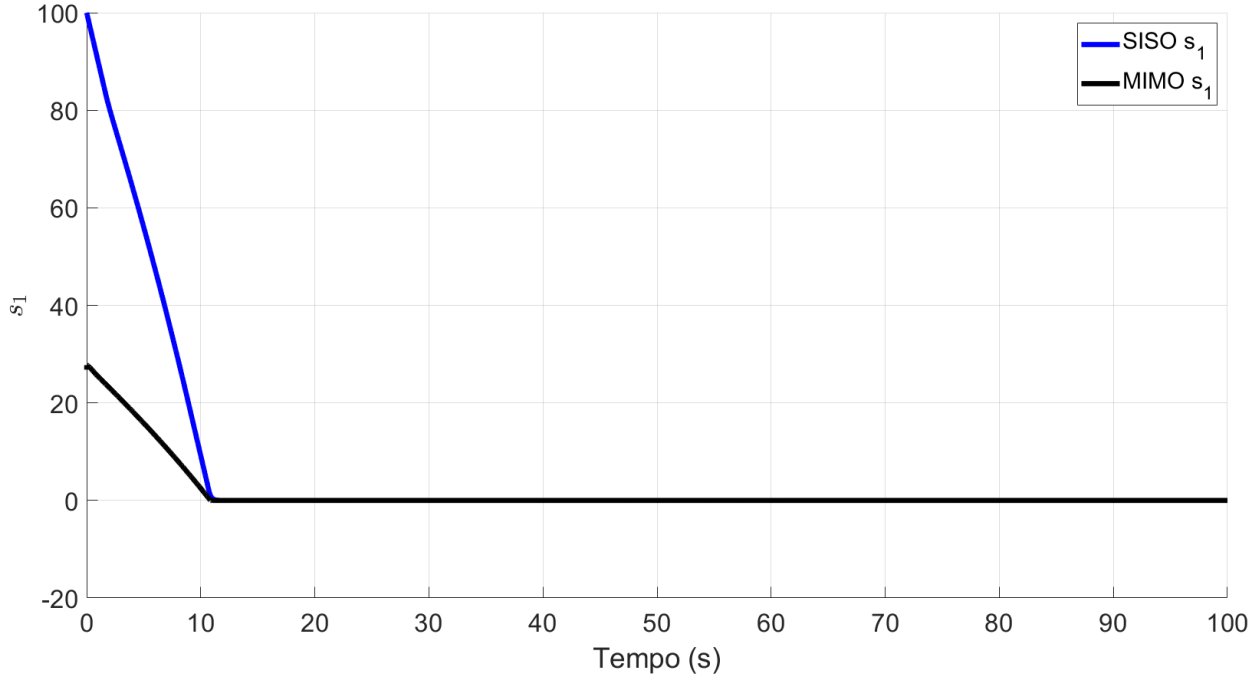

Figure 7. Comparison of the first sliding surface designed with the both techniques.

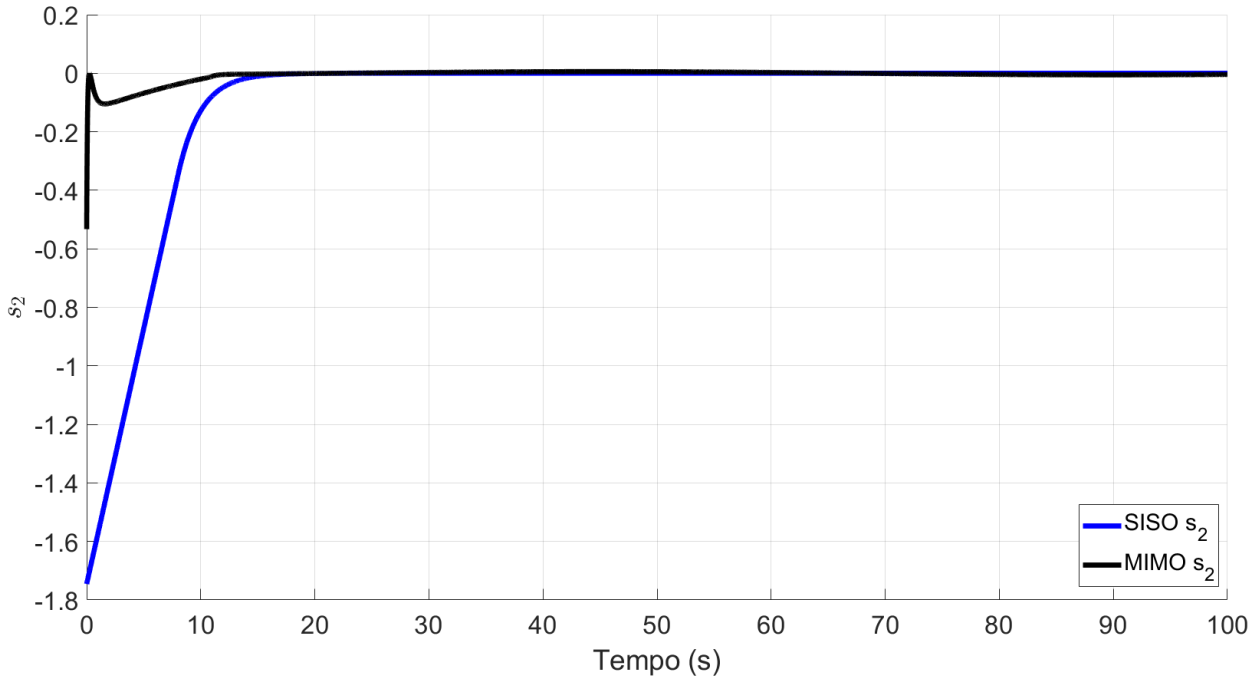

Figure 8. Comparison of the second sliding surface designed with the both techniques.

Ferreira, C.Z., CONTE, G.Y.C., AVILA, J.P.J., RIBEIRO, T.M.C. and Pereira, C., 2014. "Identification of hydrodynamic parameters for a hybrid ROV in a free-flying movement". In *International Ocean and Polar Engineering Conference (ISOPE), 2014, Busan. Proceedings of the Twenty-fourth (2014) International Ocean and Polar Engineering Conference,*. pp. 363–370. ISSN 1098-6189.

Hsu, K.C., 1998. "Variable structure control design for uncertain dynamic systems with sector nonlinearities". *Automatica*, Vol. 34, No. 4, pp. 505 – 508. doi:http://dx.doi.org/10.1016/S0005-1098(97)00233-1.

Khadhraoui, A., Beji, L., Otmane, S. and Abichou, A., 2016. "Stabilizing control and human scale simulation of a submarine ROV navigation". *Ocean Engineering*, Vol. 114, pp. 66–78. ISSN 00298018. doi: 10.1016/j.oceaneng.2015.12.054.

Meza, M., 1999. *Sliding variety design for linear multivariate systems. (In Portuguese)*. Dissertation (masters in electrical engineering).

Meza, M. and Bhaya, A., 2001. "Zero-placement approach to the design of sliding surfaces for linear multivariable systems". *Control Theory and Applications, IEEE Proceedings*, Vol. 148, No. 5, pp. 333–339. ISSN 1350-2379. doi:10.1049/ip-cta:20010680.

Ramírez-rodríguez, H., Parra-vega, V. and Sánchez-orta, A., 2017. "Fractional Sliding Mode Control of Underwater ROVs Subject to Non- differentiable Disturbances". Vol. 15, No. 3, pp. 1314–1321.

Slotine, J. and Li, W., 1991. *Applied Nonlinear Control*. Prentice Hall. ISBN 9780130408907.

Utkin, V., Guldner, J. and Shijun, M., 1999. *Sliding Mode Control in Electro-mechanical Systems*. Automation and Control Engineering. Taylor & Francis. ISBN 9780748401161.

Utkin, V. and Young, K., 1978. "Methods for constructing discontinuous planes in multidimensional variable structure systems". *Automation and Remote Control*, Vol. 31, pp. 1466–1470.

Yoerger, D. and Slotine, J.J., 1985. "Robust trajectory control of underwater vehicles". *Oceanic Engineering, IEEE Journal of*, Vol. 10, No. 4, pp. 462–470. ISSN 0364-9059. doi:10.1109/JOE.1985.1145131.

Young, K.K., Kokotovic, P. and Utkin, V., 1977. "A singular perturbation analysis of high-gain feedback systems". *IEEE Transactions on Automatic Control*, Vol. 22, No. 6, pp. 931–938. ISSN 0018-9286. doi:10.1109/TAC.1977.1101661.

7. RESPONSIBILITY NOTICE

The authors are the only responsible for the printed material included in this paper.